This is a preprint, the final version is subject to change, of the American Mineralogist (MSA)
Cite as Authors (Year) Title. American Mineralogist, in press.
DOI: http://dx.doi.org/10.2138/am-2018-6135

Revision 1

High-pressure phase transitions in $MgCr_2O_4$·Mg_2SiO_4 composition: Reactions between olivine and chromite with implications for ultrahigh-pressure chromitites

Masaki Akaogi[1*], Airi Kawahara[1], Hiroshi Kojitani[1], Kazuaki Yoshida[1], Yuki Anegawa[1], Takayuki Ishii[1]

[1]Department of Chemistry, Gakushuin University, Mejiro, Toshima-ku, Tokyo 171-8588, Japan

*Corresponding author: Masaki Akaogi

E-mail: masaki.akaogi@gakushuin.ac.jp

Phone: +81-3-3986-0221

Fax: +81-3-5992-1029

Submitted: Am. Mineral., March, 2017.

Revised: June, 2017.

This is a preprint, the final version is subject to change, of the American Mineralogist (MSA)
Cite as Authors (Year) Title. American Mineralogist, in press.
DOI: http://dx.doi.org/10.2138/am-2018-6135

Abstract

Phase relations in the Mg_2SiO_4–$MgCr_2O_4$ system were investigated in the pressure range of 9.5-27 GPa at 1600 °C to examine the possible deep mantle origin of ultrahigh-pressure (UHP) chromitites in ophiolites. The experimental results indicate that $MgCr_2O_4$-rich chromite (Ch) coexists with Mg_2SiO_4-rich olivine (Ol) below ~13.5 GPa in the equimolar Mg_2SiO_4·$MgCr_2O_4$ composition. Above ~13.5 GPa, they react to form a three-phase assemblage: garnet (Gt) solid solution in the $Mg_4Si_4O_{12}$–$Mg_3Cr_2Si_3O_{12}$ system, modified ludwigite (mLd)-type $Mg_2Cr_2O_5$ phase and $Mg_{14}Si_5O_{24}$-rich anhydrous phase B (Anh-B). At ~19.5 GPa, Anh-B is replaced by Mg_2SiO_4-rich wadsleyite (Wd). At 22 GPa, $MgCr_2O_4$-rich calcium titanate (CT) phase coexists with Mg_2SiO_4-rich ringwoodite (Rw). The assemblage of CT + Rw changes to CT + $MgSiO_3$-rich bridgmanite (Brg) + MgO periclase at 23 GPa. These sequential phase changes indicate that Ch + Ol do not directly transform to CT + Rw but to the three-phase assemblage, Gt + mLd + Anh-B (or Wd), that becomes stable at pressures corresponding to the upper and middle parts of the mantle transition zone. Our results suggest that the UHP chromitites that have been studied so far did not reach transition zone depths during mantle recycling processes of the chromitites, because there is no

evidence of the presence of the reaction products of Ol and Ch. If the reaction products, in particular mLd and Anh-B, are found in the UHP chromitites, they are good indicators to estimate the subduction depth of the chromitites.

Keywords: ultrahigh-pressure chromitite, modified ludwigite, anhydrous phase B, chromite, high pressure, phase relation, mantle transition zone, mantle recycling

Introduction

Podiform chromitites mainly comprise chromite and olivine enveloped by dunite and form pod-like bodies. Podiform chromitites are typically found in mantle peridotites in ophiolites and are regarded as products of the reaction between peridotite and melt at shallow levels of the upper mantle (Arai, 1997; Arai and Miura, 2016). However, high-pressure minerals, including diamond and coesite, were discovered in podiform chromitites in the Luobusa ophiolite in Tibet and in the Ray-Iz ophiolite in the Polar Urals (Robinson et al., 2004; Yamamoto et al., 2009; Yang et al., 2007, 2015). These discoveries suggest that these podiform chromitites, called "ultrahigh-pressure (UHP) chromitites", were derived from much deeper mantle than other podiform chromitites that formed in the shallow upper mantle. Yamamoto et al. (2009) found needle-shaped exsolution lamellae of diopsidic clinopyroxene and coesite in chromite crystals of podiform chromitites in the Luobusa ophiolite, which suggests the high solubility of SiO_2 and CaO in the host chromites. Yamamoto et al. (2009) thereby proposed that the UHP chromitites in the Luobusa ophiolite were derived from the depths >380 km, that is very close to or within the mantle transition zone, and that calcium-ferrite

(CF)-structured precursors of chromites transformed to spinel-type chromites during the transport to the upper mantle and exsolved clinopyroxene and coesite at shallow levels of the upper mantle. Their proposal is mostly based on results from diamond anvil cell experiments by Chen et al. (2003) who reported that natural Fe-rich (Fe, Mg)Cr_2O_4 chromite transformed to a CF phase above ~12.5 GPa and further to a calcium-titanate (CT) phase above ~20 GPa at ~2000 °C. The proposal is also based on Yamamoto et al.'s interpretation of high-pressure experimental results on the solid solubility of CaO and SiO_2 components in CF-type $MgAl_2O_4$ reported by Akaogi et al. (1999) and Kojitani et al. (2007). Recently, Zhang et al. (2016) discovered moissanite (SiC) as inclusions in olivine and FeNi alloys and native Si and Fe as inclusions in chromite and olivine in the Luobusa ophiolite, suggesting a highly reducing environment.

The above-mentioned petrological discoveries and interpretation have led to the inference of mantle recycling of the UHP chromitites, which were transported from the shallow upper mantle to the mantle transition zone, perhaps to the lower mantle, and returned to the earth's surface (Arai, 2010, 2013). Liou et al. (2014), Griffin et al. (2016), and Zhang et al. (2016) also advocated recycling of crustal rocks and ophiolitic peridotites in the deep upper mantle and mantle transition zone.

The mantle recycling models for the UHP chromitites described above would be

based on several assumptions. The first one is that chromite directly transforms to a CF phase without any intervening phases, similar to olivine, which directly transforms to wadsleyite at high pressure and high temperature. The second assumption is that no reaction occurs between chromite and the surrounding olivine; they separately transform to individual high-pressure phases at the P-T conditions of the mantle transition zone.

With respect to the first assumption, high-pressure phase transition studies of $MgCr_2O_4$ and $FeCr_2O_4$ indicate that, in both the compositions at 1100-1600 °C, spinel-type chromite phases first dissociate into modified ludwigite (mLd)-type $A_2Cr_2O_5$ (A = Mg, Fe) + Cr_2O_3 eskolaite (Es) with corundum structure at 13-15 GPa; the two-phase assemblage then changes into a CF or CT phase at 16-19 GPa (Ishii et al., 2014, 2015). The structure of mLd-type $A^{2+}{}_2B^{3+}{}_2O_5$ (space group *Pbam*) consists of a framework of octahedral $(B^{3+},A^{2+})O_6$ chains with tunnel-like spaces that accommodate A^{2+} cations. The structure was first determined for the high-pressure phase of $Mg_2Al_2O_5$ by Enomoto et al. (2009). In the mLd structure, A^{2+} is in the six-oxygen-coordinated trigonal prism site, while boron is two-dimensionally coordinated by three oxygen atoms in mineral ludwigite $(Mg,Fe^{2+})_2(Fe^{3+},Al)(BO_3)O_2$ (Enomoto et al., 2009). As discussed by Ishii et al. (2014, 2015), the decomposition of $MgCr_2O_4$ and $FeCr_2O_4$ chromites suggests that chromites in UHP chromitites do not directly transform to a CF

or CT phase, which might limit the depth of mantle recycling of the UHP chromitites, because mLd-type $A_2Cr_2O_5$ has not been found in nature.

With respect to the second assumption described above, it is important to investigate if reactions occur or not in the olivine-chromite system at high P-T conditions in order to apply the results to mantle recycling models regarding the origin of the UHP chromitites. Most of chromite and olivine in the podiform chromitites of the Luobusa ophiolite have typically compositions of $(Mg_{0.97},Fe_{0.03})_2SiO_4$ and $(Mg_{0.8},Fe^{2+}_{0.2})$ $(Cr_{0.75},Al_{0.2},Fe^{3+}_{0.05})_2O_4$, respectively (e.g., Yamamoto et al., 2009; Zhang et al., 2016). Therefore, the most abundant components of chromite and olivine are $MgCr_2O_4$ and Mg_2SiO_4, respectively.

In this study, we examined the phase relations in the system Mg_2SiO_4–$MgCr_2O_4$ at pressure of 9.5-27 GPa and temperature of 1600 °C. To examine possible reactions between $MgCr_2O_4$ magnesiochromite and Mg_2SiO_4 forsterite at high pressure and high temperature in detail, we used the middle composition of the system, Mg_2SiO_4:$MgCr_2O_4$ = 1:1 (molar ratio), for most of the experiments. Considering effects of minor components other than MgO, Cr_2O_3 and SiO_2, the obtained phase relations are applied to discuss mantle recycling models for the UHP chromitites. In the following sections, the spinel-type phase of pure $MgCr_2O_4$ is called magnesiochromite, while the

125 spinel-type $MgCr_2O_4$-rich phase is called chromite.

126

127 **Experimental methods**

128

129 Two types of starting materials were used for high-pressure and high-temperature
130 experiments. The first type was a mixture of synthetic Mg_2SiO_4 forsterite and $MgCr_2O_4$
131 magnesiochromite with a molar ratio of 1:1. The second starting material was a mixture
132 of MgO (> 99.9 % purity, Wako Co.), SiO_2 (> 99 %, Kanto Kagaku Co.) and Cr_2O_3 (>
133 99 %, Kanto Kagaku Co.); a mixture of MgO, SiO_2 and Cr_2O_3 with a molar ratio of
134 3:1:1 was used for the runs of 50mol%Mg_2SiO_4·50mol%$MgCr_2O_4$ composition.
135 Mixtures of MgO, SiO_2 and Cr_2O_3 with molar ratios of 19:9:1 and 13:3:7 were used for
136 the runs of 90mol%Mg_2SiO_4·10mol%$MgCr_2O_4$ and 30mol%Mg_2SiO_4·70mol%$MgCr_2O_4$
137 respectively. Mg_2SiO_4 forsterite was prepared from a 2:1 molar mixture of MgO and
138 SiO_2 by heating in air at 1500 °C for 46 h. $MgCr_2O_4$ magnesiochromite was synthesized
139 from MgO and Cr_2O_3 with 1:1 molar ratio by heating at 1300 °C for 24 h under CO_2 gas
140 flow. Powder X-ray diffraction measurements indicated that the forsterite and
141 magnesiochromite were single-phase materials with olivine and spinel structures,
142 respectively. The lattice parameters determined by powder X-ray diffraction were a =

143 5.9811(1) Å, b = 10.2004(3) Å, and c = 4.7558(1) Å for Mg_2SiO_4 forsterite and a =
144 8.3303(2) Å for $MgCr_2O_4$ magnesiochromite; they were in excellent agreement with
145 those repotrted in Kirfel et al. (2005) and Lenaz et al. (2004), respectively.

146 High-pressure and high-temperature experiments were performed using a
147 Kawai-type 6-8 multianvil apparatus at Gakushuin University. Tungsten carbide anvils
148 with 2.5 mm truncated edge length were used in combination with a 5 wt%
149 Cr_2O_3-doped MgO octahedron with 7 mm edge length as the pressure medium. A
150 tubular Re heater was placed in the central part of the octahedron. The powdered
151 starting material was put into the Re heater. A $LaCrO_3$ sleeve was placed between the
152 furnace and the MgO octahedron for thermal insulation; two $LaCrO_3$ end-plugs were
153 inserted into both ends of the furnace. Two thin Pt discs were placed between the
154 starting material and end-plugs to avoid reaction between them. In some runs, a Pt
155 capsule containing the starting material was placed into the Re heater, and a BN sleeve
156 was inserted between the capsule and furnace for electrical insulation. Temperature was
157 measured at the central part of the outer surface of the furnace using a Pt/Pt-13%Rh
158 thermocouple. No correction was made with respect to the effect of pressure on the
159 electromotive force of the thermocouple.

160 Pressure was calibrated at room temperature using the transitions of Bi I-II (2.55

GPa), Bi III-V (7.7GPa), ZnS (15.6 GPa) and GaAs (18.3 GPa) by Ito (2007) and that of GaP (23 GPa) by Dunn and Bundy (1978). The pressure was further calibrated at 1600 °C, using coesite–stishovite transition in SiO_2 (Zhang et al., 1996), rutile–αPbO_2 transition in TiO_2 (Withers et al., 2003), olivine–wadsleyite and wadsleyite–ringwoodite transitions in Mg_2SiO_4 (Morishima et al., 1994; Suzuki et al., 2000), and akimotoite–bridgmanite transition in $MgSiO_3$ (Fei et al., 2004). The experimental errors in pressure and temperature were estimated to be within ±0.3 GPa and ±20 °C, respectively. The samples were kept at 9.5-27 GPa and 1600 °C for 180-360 min, quenched under pressure, and recovered to 1 atm.

The recovered run products were mounted on glass slides using epoxy resin and polished to expose the samples for phase identification and composition analysis. A microfocus X-ray diffractometer (Rigaku, RINT2500, MDG) with a rotating anode operated at 45 kV and 250 mA was used for phase identification. The X-ray beam was collimated to 50 μm in diameter. For the texture observation and composition analysis of the polished samples, a scanning electron microscope (SEM, JEOL JMS-6360) operated at an acceleration voltage of 15 kV and probe current of 0.58 nA was used, in combination with an energy-dispersive X-ray spectrometer (EDS, SGX Sensortech Sirius SD-10133). As the standard materials, synthetic Cr_2O_3 eskolaite was used for Cr,

and synthetic $MgSiO_3$ enstatite (Ozima, 1982) for Mg and Si.

Results and discussion

Phase changes in the Mg_2SiO_4–$MgCr_2O_4$ system

The results of the high-pressure experiments in the Mg_2SiO_4–$MgCr_2O_4$ system are summarized in Table 1. Phase identification was made by both microfocus X-ray diffraction and composition analysis with SEM-EDS. Typical microfocus X-ray diffraction patterns of the run products are shown in Figs. 1 and 2; the backscattered electron images of the run products are displayed in Fig. 3. The compositions of coexisting phases are listed in Table 2, and plotted in triangular diagrams of the system MgO–SiO_2–Cr_2O_3 in Fig. 4. The molar volumes of endmember phases in the system MgO–SiO_2–Cr_2O_3 are summarized in Table 3; a detailed explanation of some of the data in Table 3 is described later.

The X-ray diffraction patterns of the run products at 9.5-12.5 GPa and 1600 °C show that the coexisting phases are olivine (Ol) and chromite (Ch) (Fig. 1a). Table 2 and Fig. 4b represent the compositions of Ol and Ch in the system MgO–SiO_2–Cr_2O_3. In this pressure range, the Ch compositions in Table 2 indicate that 6.2-7.9 mol %

Mg_2SiO_4 component is dissolved into Ch, while Ol contains only ~1-2 wt % Cr_2O_3. To examine if the compositions were in equilibrium, we carried out experiments at 12.5 GPa and 1600 °C for the run durations of 3 and 6 h (A140704 and K160113). Tables 1 and 2 indicate that the run products consisted of the same mineral assemblage with very similar compositions, confirming that the products were close to equilibrium.

At pressure between 12.5 and 14 GPa, the phase assemblage of Ol + Ch drastically changes into a three-phase assemblage, garnet (Gt) + modified ludwigite (mLd) phase + anhydrous phase B (Anh-B):

$$\text{Ol} + \text{Ch} \rightarrow \text{Gt} + \text{mLd} + \text{Anh-B} \quad (1)$$

Based on the microfocus X-ray diffraction and SEM-EDS analyses, this assemblage is stable at the pressure range of about 14-19 GPa. Fig. 1b shows that most of the diffraction peaks of the run product are assigned to Gt, mLd and Anh-B. Anh-B was identified based on six diffraction peaks not overlapping with that of other phases and additional three peaks overlapping with that of other phases. The compositions in Table 2 also indicate the presence of Anh-B in the run products at 14-19 GPa. Bindi et al. (2016) synthesized single crystals of Anh-B in the Mg_2SiO_4–$MgCr_2O_4$ system at similar

215 P-T conditions, and made the structure refinement. Anh-B is a high-pressure magnesium
216 silicate with $Mg_{14}Si_5O_{24}$ composition as the Mg-endmember, which is stable above
217 11-13 GPa at 1300-1600 °C (Ganguly and Frost, 2006; Kojitani et al., 2017). The
218 structure of Anh-B consists of two-types of layers: rock-salt-type layers with
219 edge-sharing $(Mg,Si)O_6$ octahedra and forsterite-type layers with MgO_6 octahedra and
220 SiO_4 tetrahedra (Finger et al., 1991).

221 Table 2 and Fig. 4c show the compositions of Gt, mLd and Anh-B of the runs at
222 14-19 GPa. The mLd phase has a composition close to $Mg_2Cr_2O_5$, while Anh-B contains
223 12-20 wt% Cr_2O_3 due to the substitution of Mg^{2+} and Si^{4+} for 2 Cr^{3+}. The compositions
224 of Gt at 14-19 GPa indicate the formation of garnet solid solutions between $Mg_4Si_4O_{12}$
225 (majorite, Mj) and $Mg_3Cr_2Si_3O_{12}$ (knorringite, Kn); the proportion of Kn is larger than
226 that of Mj. To examine if the run products were in equilibrium, we carried out two runs
227 for 3 and 6 h at 14 GPa and 1600 °C (A140801 and Y161025). Both run products
228 consisted of Gt, mLd and Anh-B (Table 1) and have very similar compositions (Table 2).
229 This confirms again that the run products were close to equilibrium.

230 The phase changes from Ol + Ch to Gt + mLd + Anh-B can be approximated by the
231 following reaction:

232

233 $37Mg_2SiO_4(Ol) + 37MgCr_2O_4(Ch) \rightarrow 9Mg_3Cr_2Si_3O_{12}(Kn) + 28Mg_2Cr_2O_5(mLd) +$

234 $2Mg_{14}Si_5O_{24}(Anh\text{-}B)$ (2)

235

236 This reaction probably occurs due to the instability of $MgCr_2O_4$ Ch relative to mLd + Es

237 (Cr_2O_3) at pressure above ~13 GPa at 1600 °C (Ishii et al., 2015), and the Cr_2O_3 product

238 reacts with Mg_2SiO_4 and Gt and Anh-B are formed. The density increase of the reaction

239 in Equation 2 was calculated to be 7.2 % at ambient conditions, using the data in Table 3.

240 The pressure of the transition from Ol + Ch to Gt + mLd + Anh-B is very close to the

241 lower stability limit (13 GPa at 1600 °C) of $Mg_{14}Si_5O_{24}$ Anh-B determined in our study

242 (Kojitani et al., 2017).

243 The assemblage of Gt + mLd + Anh-B changes to Gt + mLd + Wd at pressure

244 between 19 and 20.5 GPa at 1600 °C:

245

246 $Gt + mLd + Anh\text{-}B \rightarrow Gt + mLd + Wd$ (3)

247

248 Although the X-ray diffraction patterns of Anh-B and Wd are similar, the diffraction

249 peaks characteristic for Anh-B at 2θ of 66-68° and 102-103° diminish and a peak of Wd

250 not overlapping with that of other phases appears at ~105° in Fig. 2a of the run product

at 20.5 GPa and 1600 °C. The diffraction profile suggests that Wd is present in the sample rather than Anh-B. The compositions in Table 2 clearly indicate that the analyzed phase is Wd; it contains 5.3 mol% $MgCr_2O_4$ component and coexists with Gt and mLd. The relatively weak diffraction peaks of Wd in Fig. 2a agree with the small abundance indicated in Fig. 3c. Table 2 shows that $Mg_4Si_4O_{12}$ (Mj) component in Gt synthesized at 14-20.5 GPa increases with increasing pressure. This is consistent with the stability field of Gt, which expands to the $Mg_4Si_4O_{12}$-rich side with pressure in the system $Mg_4Si_4O_{12}$–$Mg_3Cr_2Si_3O_{12}$ (Sirotkina et al., 2015). The pressure of the phase change in Equation 3 is consistent with the upper stability limit (19 GPa at 1600 °C) of $Mg_{14}Si_5O_{24}$ Anh-B determined in our study (Kojitani et al., 2017). The phase changes of Equation 3 may be expressed by the following reaction, keeping the bulk Mg_2SiO_4·$MgCr_2O_4$ composition:

$$9Mg_3Cr_2Si_3O_{12}(Kn) + 28Mg_2Cr_2O_5(mLd) + 2Mg_{14}Si_5O_{24}(Anh\text{-}B) \rightarrow$$
$$5Mg_3Cr_2Si_3O_{12}(Kn) + 3Mg_4Si_4O_{12}(Mj) + 32Mg_2Cr_2O_5(mLd) + 10Mg_2SiO_4(Wd) \quad (4)$$

The density increase of the reaction in Equation 4 is 0.7 %.

At pressure between 20.5 and 21.5 GPa, Wd transforms to ringwoodite (Rw), and Gt

and mLd react to form Rw and CT; therefore, only Rw and CT coexist in the sample (Figs. 2b and 3d). The whole reaction is expressed by:

$$Gt + mLd + Wd \rightarrow Rw + CT \quad (5)$$

The compositions of Rw and CT in Table 2 and Fig. 4e show that the proportion of Mg_2SiO_4 component in CT increases substantially from 6.0 to 15.0 mol% and that of $MgCr_2O_4$ in Rw increases from 1.5 to 5.8 mol% between 21.5 and 22.5 GPa,. The phase change of Equation 5 can be expressed by the two following reactions in which Kn and Mj are involved separately:

$$2Mg_2SiO_4(Wd) + Mg_3Cr_2Si_3O_{12}(Kn) + 4Mg_2Cr_2O_5(mLd) \rightarrow 5Mg_2SiO_4(Rw) + 5MgCr_2O_4(CT) \quad (6)$$

$$Mg_4Si_4O_{12}(Mj) + 4Mg_2Cr_2O_5(mLd) \rightarrow 4Mg_2SiO_4(Rw) + 4MgCr_2O_4(CT) \quad (7)$$

The density increase of the reactions in Equations 6 and 7 is 2.6 and 1.4 %, respectively.

At pressure between 22.5 and 24 GPa, Rw dissociates into perovskite-structured

bridgmanite (Brg) and periclase (Per):

$$Rw + CT \rightarrow Brg + Per + CT \quad (8)$$

Per was observed in the microfocus X-ray diffraction pattern (Fig. 2c) and in the backscattered electron image of Fig. 3e where small, highly MgO-rich grains were identified as Per. Reliable chemical analysis of Per was difficult, because the grain size of Per was generally very small (< 3 μm). Therefore, we assume that Per is pure MgO. Brg contains 5.4-7.2 wt% Cr_2O_3 due to the substitution of Mg^{2+} and Si^{4+} for 2 Cr^{3+}. The Cr_2O_3 content of Brg is comparable with that synthesized at 23 GPa by Bindi et al. (2014). CT contains a substantial Mg_2SiO_4 component of about 18-20 mol% at 24-27 GPa. While keeping the bulk Mg_2SiO_4·$MgCr_2O_4$ composition, this reaction can be approximated by the equation:

$$Mg_2SiO_4(Rw) + MgCr_2O_4(CT) \rightarrow MgSiO_3(Brg) + MgO(Per) + MgCr_2O_4(CT) \quad (9)$$

The density increase of the reaction in Equation 9 is 5.1 %. The three-phase assemblage of Brg + Per + CT is stable up to at least 27 GPa.

We carried out additional runs at 15 GPa and 1600 °C for the following compositions: 90mol%Mg_2SiO_4·10mol%$MgCr_2O_4$ and 30mol%Mg_2SiO_4·70mol%$MgCr_2O_4$ (Y160117 and Y160119). The run product in the former composition was Gt + Anh-B + Wd, and that in the latter was Gt + mLd + Es. Based on the assemblage of Gt + mLd + Anh-B that was observed at 14 GPa and 1600 °C for the composition of 50mol%Mg_2SiO_4·50mol%$MgCr_2O_4$, it is concluded that the assemblage of Ol + Ch destabilizes at about 13-14 GPa in the Mg_2SiO_4–$MgCr_2O_4$ system and changes to the assemblage containing Gt + mLd and/or Anh-B.

Wu et al. (2016) recently determined phase relations using a starting material of 90wt% natural chromite $(Mg_{0.79},Fe^{2+}_{0.21})_{1.00}(Al_{0.42},Cr_{1.50},Fe^{3+}_{0.10})_{1.98}O_4$ + 10wt% SiO_2 at 5-15 GPa and 1000-1600 °C. Their experimental results indicate that Ch + Gt + Es coexist at 12-14 GPa at 1600 °C; the assemblage changes to mLd + Gt + Es at 15 GPa. The Gt phases contain both Mj and Kn components. The composition of Ch–SiO_2 system studied by Wu et al. (2016) can be approximated as MgO:SiO_2:Cr_2O_3 = 42.5:15.0:42.5 (molar ratios) in the MgO–SiO_2–Cr_2O_3 system, ignoring minor concentrations of Fe^{2+}, Al^{3+} and Fe^{3+} in Ch. The small open diamond symbols in Figs. 4b and 4c indicate the approximate composition. Fig. 4b shows that the phase assemblage of Ch + Gt + Es reported in Wu et al. (2016) is consistent with Ol + Ch in

323 the Mg_2SiO_4–$MgCr_2O_4$ system of our study, because all the phases (Ol, Ch, Gt and Es)
324 are stable in the pressure range of 10-12 GPa. Furthermore, the assemblage of mLd + Gt
325 + Es at 15 GPa in Wu et al.'s (2016) study is the same as the coexisting phases at the
326 same pressure in 30mol%Mg_2SiO_4·70mol% $MgCr_2O_4$ composition in our study (Table
327 1).
328
329 **Changes in mineral proportions with pressure**
330 With the pressure increase from 9.5 to 27 GPa, the mineral assemblage of the
331 Mg_2SiO_4·$MgCr_2O_4$ composition changes from Ol + Ch to Brg + Per + CT, and the three
332 different phase assemblages intervene between Ol + Ch and Brg + Per + CT, as
333 described above. We determined the mineral proportions (vol%) in the pressure range of
334 9.5-27 GPa by mass balance calculations (Herrmann and Berry, 2002), using the
335 compositions of Table 2. Based on the calculated mineral proportions, we evaluated the
336 densities of the mineral assemblages at ambient conditions. For both the calculations of
337 mineral proportions and densities, we used the molar volume data of Table 3. The
338 elastic properties and thermal expansivities of several high-pressure phases, particularly
339 mLd, CT and Mj-Kn garnet solid solutions, have not been measured, or are poorly
340 constrained. Therefore, the densities were only calculated for ambient conditions. The

molar volume of $Mg_4Si_4O_{12}$ (Mj) in Table 3 was estimated by extrapolating the lattice parameters of cubic garnet solid solutions in the system $Mg_4Si_4O_{12}$–$Mg_3Al_2Si_3O_{12}$ (Heinemann et al., 1997). Similarly, the molar volume of $Mg_3Cr_2Si_3O_{12}$ (Kn) was estimated by the extrapolation of cell parameters of cubic garnet solid solutions in the system $Mg_4Si_4O_{12}$–$Mg_3Cr_2Si_3O_{12}$, although pure $Mg_3Cr_2Si_3O_{12}$ garnet is not stable in the whole pressure range studied (Sirotkina et al., 2015). We also assumed that the molar volume of the hypothetical endmember of CT-type Mg_2SiO_4 is the same as that of CF-type Mg_2SiO_4 estimated by Kojitani et al. (2007), because the volume difference between CT and CF phases is very small (Ishii et al., 2014). With respect to the calculations of the mineral proportions and densities, effects of the incorporation of small amounts of Cr_2O_3 in Brg and Anh-B were corrected using the volume data of Cr-bearing Brg and Anh-B reported in Bindi et al. (2014, 2016). We assumed that the effect of Cr_2O_3 dissolution on the volume of Wd is the same as that of Rw and that mLd and Per have $Mg_2Cr_2O_5$ and MgO composition, respectively (Table 2).

Figure 5 shows the calculated mineral proportions in the bulk Mg_2SiO_4·$MgCr_2O_4$ composition as a function of pressure at 1600 °C. With increasing pressure, the phase assemblage changes: Ol + Ch → Gt + Anh-B + mLd → Gt + Wd + mLd → Rw + CT → Brg + Per +CT. The gray zones in Fig. 5 show narrow pressure ranges in which the

359 transitions occur; detailed phase relations in the ranges have not been examined. The
360 proportions of minerals are generally consistent with those estimated based on Figs. 3
361 and 4. The effects of pressure on the mineral proportions are generally small for each
362 mineral assemblage (Fig. 5). The change in the proportions of CT and Rw with pressure
363 corresponds to the increase of Mg_2SiO_4 solubility in CT at 21.5-22.5 GPa, as described
364 above. It should be noted that Fig. 5 indicates that Ol + Ch do not directly transform to
365 Rw + CT but the assemblages of Gt + mLd + Anh-B and Gt + mLd + Wd are stable at
366 about 13.5-21 GPa.

367 Based on the mineral proportions and phase compositions, the densities of the phase
368 assemblages at ambient conditions are: 3.84 g/cm^3 for Ol + Ch, 4.10 g/cm^3 for Gt +
369 Anh-B + mLd, 4.12 g/cm^3 for Gt + Wd + mLd, 4.23 g/cm^3 for Rw + CT, and 4.43 g/cm^3
370 for Brg + Per +CT. These density increases accompanying the phases changes are
371 compatible with the density increases of the simplified reactions of Equations 2, 4, 6, 7
372 and 9.

373

374 **Effects of minor components on phase relations**

375 To apply the phase relations in the Mg_2SiO_4–$MgCr_2O_4$ system to natural UHP
376 chromitites, it is necessary to discuss the effects of minor components other than MgO,

Cr_2O_3 and SiO_2 on the phase relations. Chromites in the UHP chromitites contain small amounts of FeO ($Fe^{2+}/(Mg+Fe^{2+}) \approx 0.2$) and Al_2O_3 ($Al/(Cr+Al) \approx 0.2$), as described in the Introduction. To evaluate the effect of FeO, we compared the phase relations of $MgCr_2O_4$ with those of $FeCr_2O_4$. At 1400-1600 °C, $MgCr_2O_4$ Ch dissociates into mLd-type $Mg_2Cr_2O_5$ + Cr_2O_3 (Es) at 12-13 GPa, which combine to CT-type $MgCr_2O_4$ at 16-17 GPa (Ishii et al., 2015). At 1400-1600 °C, $FeCr_2O_4$ Ch decomposes to mLd-type $Fe_2Cr_2O_5$ + Es at 12.5-13 GPa, which change to CT-type $FeCr_2O_4$ at 16-18 GPa, but combine to CF-type $FeCr_2O_4$ below ~1400 °C (Ishii et al., 2014). These experimental data indicate that the transition pressures of $FeCr_2O_4$ are very close to those of $MgCr_2O_4$, taking into account the structural similarity between CF and CT. Therefore, we infer that a substitution of Mg^{2+} by Fe^{2+} of ~20 mol % has minor effects on the phase relations of the Mg_2SiO_4–$MgCr_2O_4$ system.

To examine the effects of Al_2O_3, we compared our results on high-pressure phase transitions of $MgAl_2O_4$ spinel (Sp) (Kojitani et al., 2010) with those of $MgCr_2O_4$ Ch (Ishii et al., 2015). $MgAl_2O_4$ Sp dissociates into mLd-type $Mg_2Al_2O_5$ and Al_2O_3 corundum at ~20 GPa above ~2000 °C, while Sp decomposes into MgO + Al_2O_3 below ~2000 °C. Both of the decomposed phase assemblages change to $MgAl_2O_4$ CF at around 26 GPa. The comparison of the phase transitions of $MgAl_2O_4$ with those of

395 $MgCr_2O_4$ suggests that a substitution of Cr^{3+} by Al^{3+} of ~20 mol % in Ch might slightly
396 increase the transition pressure and temperature.

397 We also compared our phase relations in the Mg_2SiO_4–$MgCr_2O_4$ system with that of
398 the natural Ch–silica system by Wu et al. (2016). As described above, their results for
399 the composition of 90wt% $(Mg_{0.79},Fe^{2+}_{0.21})_{1.00}(Al_{0.42},Cr_{1.50},Fe^{3+}_{0.10})_{1.98}O_4$ Ch + 10wt%
400 SiO_2 indicate that the assemblage of Ch + Gt + Es changes to that of mLd + Gt + Es at
401 14-15 GPa and 1600 °C. The pressure is close to that of our study (12.5-14 GPa) at
402 which Ol + Ch changes to Gt + mLd + Anh-B in the Mg_2SiO_4–$MgCr_2O_4$ system. The
403 comparable pressure of the upper stability limit of Ch suggests that small amounts of
404 Al_2O_3 and SiO_2 barely affect on the phase relations.

405 Some of the UHP chromitites contain small amounts of diopside (Di) (e.g., Zhang et
406 al., 2016; Griffin et al., 2016). Zhang et al. (2017) studied the phase relations at 12-21
407 GPa and 1400-1600 °C in the Al-bearing Ch–Di system with compositions on the join
408 $xMg(Cr_{1.5},Al_{0.5})O_4$–$(1-x)CaMgSi_2O_6$ (x = 0.90, 0.95). Based on their results, Ch + Gt +
409 Es are stable at 12 GPa at 1600 °C. Above the pressure between 12 and 14 GPa, a CF
410 phase coexists with Ch + Gt + Es, and mLd occurs at 15-18 GPa. The CF + mLd + Gt +
411 Es assemblage changes to CT + Gt + Es at ~20 GPa. The CF phase contains ~7-8 wt%
412 CaO and ~3-5 wt% SiO_2. This suggests that the CF phase is a possible precursor of Ch

413 containing Di and coesite lamellae, because Ch with exsolution lamellae of Di and
414 coesite is commonly found in the UHP chromitites (Yamamoto et al., 2009). The CF
415 phase was not observed in our studies in the system Mg_2SiO_4–$MgCr_2O_4$. The different
416 phase relations are probably due to the presence of minor components, i.e., CaO and
417 Al_2O_3, in the system studied by Zhang et al. (2017), as discussed below.

418 The experimental results on high-pressure phase relations in the system
419 $MgAl_2O_4$–$CaAl_2O_4$ indicate that a hexagonal aluminous phase with $(Mg_{1-x},Ca_x)Al_2O_4$
420 composition ($x \approx 0.2$-0.35) becomes stable above 15 GPa at 1200 °C, instead of a
421 Ca-bearing, Mg-rich CF phase (Akaogi et al., 1999). The general formula of the
422 hexagonal phase (in this case $CaMg_2Al_6O_{12}$) is $AB_2C_6O_{12}$. The hexagonal aluminous
423 phase (also called NAL phase; space group $P6_3/m$) has a similar but different structure
424 from the CF phase (space group *Pbnm*). The structure of $CaMg_2Al_6O_{12}$ NAL phase
425 consists of double chains of AlO_6 octahedra along the c axis, and Mg ions occupy
426 six-fold prism sites and Ca in 9-fold pseudo-hexagonal tunnel sites surrounded by the
427 double chains of octahedra (Miura et al., 2000). The NAL phases with more complex
428 compositions are also stable in MORB above ~22 GPa (e.g., Sanehira et al., 2008;
429 Ricolleau et al., 2010). A NAL phase with $(Mg_{0.71},Ca_{0.26})(Al_{1.36},Si_{0.49})O_4$ composition by
430 Miyajima et al. (2001) indicates a high SiO_2 content of the phase. Raman spectra and

powder X-ray diffraction patterns of the NAL phase are very similar to those of the CF phase (Akaogi et al., 1999; Kojitani et al., 2007; Ono et al., 2009). Because the "CF phase" of Zhang et al. (2017) has an average composition of $(Mg_{0.70},Ca_{0.25})(Al_{0.41},Si_{0.13}Cr_{1.44})O_4$ with a very similar Mg:Ca ratio and the stability pressure range to that of the NAL phase in the system $MgAl_2O_4$–$CaAl_2O_4$ and shows a similar SiO_2 solubility to that in the NAL phases in the previous studies, it is likely that the "CF phase" is a NAL phase rather than CF. However, though the "CF phase" reported in Zhang et al. (2017) is in fact a NAL phase, their results indicate that the phase contains substantial amounts of CaO and SiO_2 and that it is a possible precursor for Ch containing exsolved lamellae of Di and coesite.

Implications

High-pressure minerals, such as diamond and coesite, and highly reduced phases were discovered in the UHP podiform chromitites, as described above. However, it is generally believed that podiform chromitites were formed at shallow levels of the upper mantle. To reconcile the issues on the formation of UHP podiform chromitites, subduction-recycling models of the podiform chromitites are most widely used. The

449 models are basically as follows (Arai, 2010, 2013; Griffin et al., 2016). Podiform
450 chromitites composed of Ch and Ol enveloped by dunite were formed by the reaction
451 between peridotite and magma at shallow depths of the upper mantle. The podiform
452 chromitites were subducted into the deep mantle due to mantle convection. In the
453 transition zone, Ol transformed to Wd (or Rw), and Ch changed to CF (or CT) which
454 could incorporate CaO and SiO_2 components. Subsequently, the podiform chromitites
455 with the mineral assemblage of Wd (or Rw) + CF (or CT) were transported to shallow
456 levels of the upper mantle via mantle upwelling, converted to Ol + Ch, and diopsidic
457 pyroxene and coesite were exsolved in Ch. In the models, it was postulated that the
458 initial igneous textures of the podiform chromitites were basically preserved during
459 deep mantle recycling based on the assumption that reactions between Ol and Ch and
460 between their high-pressure polymorphs did not take place (Arai, 2013; Satsukawa et al.,
461 2015).

462 Figure 5 indicates that, in the system Mg_2SiO_4–$MgCr_2O_4$, Ol and Ch react at ~13.5
463 GPa and 1600 °C, resulting in the formation of the three-phase assemblage, Gt + mLd +
464 Anh-B, which subsequently changes to Gt + mLd + Wd at ~19.5 GPa. This means that
465 Ol and Ch do not directly transform to Wd (or Rw) and CT, respectively. We infer that
466 our results in the system Mg_2SiO_4–$MgCr_2O_4$ can be applied to the UHP chromitites,

because both Ol and Ch of the UHP chromitites have Mg-rich compositions and the effects of minor components on the phase relations are small, as discussed above.

The pressure of 13.5 GPa at which Ol + Ch change to Gt + mLd + Anh-B is very close to that of the 410 km seismic discontinuity (13.7 GPa) dividing the mantle transition zone from the upper mantle. To the best of our knowledge, no petrological studies of the UHP chromitites reported evidence of the reaction between Ol and Ch, which first produces the three-phase assemblage of Gt + mLd + Anh-B. Once the reaction occurred, the product phases would have been preserved, at least in part, in the UHP chromitites.

The effect of temperature on the reaction between Ol and Ch should also be considered. Taking into account a typical low-temperature geotherm of the subduction zone (Kirby et al., 1996), the temperature of subducted podiform chromitites may be around 700-1000 °C at transition zone depths. Therefore, the reaction between Ol and Ch might be kinetically hindered or direct transitions of Ol to Wd (or Rw) and Ch to CT might occur. However, to generate buoyancy in the mantle upwelling processes, the temperature of the podiform chromitites would need to be higher than the normal geotherm, 1400-1600 °C, in the mantle transition zone (Akaogi et al., 1989). Therefore, the reaction would occur, producing the assemblage of Gt + mLd + Anh-B in the

485 upper-half of the transition zone. In our high-pressure experiments at 1600 °C for 3-6 h,
486 the grain sizes of these phases were generally in the range of ~5-20 μm (Fig. 3).
487 Considering the transition zone temperature, it is likely that grain growth to at least
488 several mm or cm would occur, given the expected timescale of the geological
489 processes. Once the reaction had occurred, it would be difficult for the phases to
490 completely react again to form Ol and Ch and to recover a similar texture to that before
491 the reaction. Therefore, a part of the reaction products would be preserved.

492 An example of such preserved phase assemblages which indicate mineral reactions
493 due to changes in the P-T conditions is "spinel-pyroxene symplectite", a reaction
494 product between Ol and plagioclase. The spinel-pyroxene symplectite in lherzolite
495 xenoliths from the Ichinomegata Crater, Oga Peninsula, northeast Japan, was studied in
496 detail by Takahashi (1986). It was concluded that the complex texture of product phases
497 (Ca-rich pyroxene, Ca-poor pyroxene and $MgAl_2O_4$-rich spinel) was formed due to the
498 reaction between Ol and plagioclase in peridotite with increasing pressure and/or
499 decreasing temperature. The reaction products between Ol and Ch have not been
500 reported in petrological studies of the UHP chromitites,. The fact that there is no
501 evidence of the presence of the mLd + Anh-B + Gt assemblage in the UHP chromitites
502 strongly suggests that the chromitites did not reach the mantle transition zone depths.

Zhang et al. (2017) suggested that the UHP chromitites were subducted to depths exceeding ~360 km (12 GPa), where the chromitites were metamorphosed and the "CF phase" containing several wt% of CaO and SiO_2 was formed. Due to the ascent of the chromitites, the "CF phase" would transform to Ch and possibly a small amount of ugrandite garnet, and Di and coesite were exsolved in Ch as lamellae. This is a possible mechanism explaining the presence of Ch containing Di and coesite lamellae in the UHP chromitites. Zhang et al. (2017) proposed that the subduction depth did not exceed ~440 km (15 GPa), because the mLd phase is not present in the chromitites, assuming that the absence of a reaction between Ol and Ch. In addition to the depth limit suggested by Zhang et al. (2017), our experimental data indicate that the UHP chromitites did not experience pressure exceeding ~13.5 GPa, which corresponds to the top (410 km depth) of the transition zone, because the reaction products of Ol and Ch, the two most abundant minerals of the UHP chromitites, have not been observed. If the reaction products, including mLd and Anh-B, will be discovered in the UHP chromitites in future, their presence can be used as a good indicator to more precisely evaluate the subduction depth of the chromitites in the transition zone.

Acknowledgments

We are grateful to S. Arai for invaluable suggestions and discussions. We also thank R. Tao and an anonymous referee for careful review and the Associate Editor for constructive comments. This work was supported in part by the JSPS grant (Nos. 25287145 and 17H02986 to M. A.) and by the MEXT-supported program for the Strategic Research Foundation at Private Universities.

References

Akaogi, M., Ito, E., and Navrotsky, A. (1989) Olivine–modified spinel–spinel transitions in the system Mg_2SiO_4–Fe_2SiO_4: Calorimetric measurements, thermochemical calculation, and geophysical application. Journal of Geophysical Research, 94, 15671–15685, doi:10.1029/JB094iB11p15671.

Akaogi, M., Hamada, Y., Suzuki, T., Kobayashi, M., and Okada, M. (1999) High pressure transitions in the system $MgAl_2O_4$-$CaAl_2O_4$: a new hexagonal aluminous phase with implication for the lower mantle. Physics of the Earth and Planetary Interiors, 115, 67-77.

539 Arai, S. (1997) Control of wall-rock composition on the formation of podiform
540 chromitites as a result of magma/peridotite interaction. Resource Geology, 47,
541 177-187.
542 Arai, S. (2010) Possible recycled origin for ultrahigh-pressure chromitites in ophiolite.
543 Journal of Mineralogical and Petrological Sciences, 105, 280-285, doi: 10.2465/
544 jmps.100622a.
545 Arai, S. (2013) Conversion of low-pressure chromitites to ultrahigh-pressure chromitites
546 by deep recycling: A good inference. Earth and Planetary Science Letters, 379, 81-87,
547 doi.org/10.1016/j.epsl.2013.08.006.
548 Arai, S., and Miura, M. (2016) Formation and modification of chromitites in the mantle.
549 Lithos, 264, 277-295.
550 Bindi, L., Sirotkina, E.A., Bobrov, A.V., and Irifune, T. (2014) Chromium solubility in
551 perovskite at high pressure: The structure of $(Mg_{1-x}Cr_x)(Si_{1-x},Cr_x)O_3$ (with x=0.07)
552 synthesized at 23 GPa and 1600 °C. American Mineralogist, 99, 866-869.
553 Bindi, L., Sirotkina, E.A., Bobrov, A.V., Nestola, F., and Irifune, T. (2016) Chromium
554 solubility in anhydrous phase B. Physics and Chemistry of Minerals, 43, 103-110.
555 DOI 10.1007/s00269-015-0777-2
556 Chen, M., Shu, J., Mao, H.K., Xie, X., and Hemley, R.J. (2003) Natural occurrence and

557 synthesis of two new postspinel polymorphs of chromite. Proceeding of the National
558 Academy of Sciences, 100, 14651-14654, doi/10.1073/pnas.2136599100.
559 Dobson, D.P., and Jacobsen, S.D. (2004) The flux growth of magnesium silicate
560 perovskite single crystals. American Mineralogist, 89, 807–811.
561 Dunn, K.J., and Bundy, F.P. (1978) Materials and techniques for pressure calibration by
562 resistance-jump transitions up to 500 kilobars. Review of Scientific Instruments, 49,
563 365-370.
564 Enomoto, A., Kojitani, H., Akaogi, M., and Yusa, H. (2009) High-pressure transitions in
565 $MgAl_2O_4$ and a new high-pressure phase of $Mg_2Al_2O_5$. Journal of Solid State
566 Chemistry, 182, 389-395, doi:10.1016/j.jssc.2008.11.015.
567 Fei, Y., Van Orman, J., Li, J., Van Westrenen, W., Sanloup, C., Minarik, W., Hirose, K.,
568 and Komabayashi, T. (2004) Experimentally determined post-spinel transformation
569 boundary Mg_2SiO_4 using MgO as an internal pressure standard and its geophysical
570 implications. Journal of Geophysical Research, 109, doi: 10.1029/2003JB002562.
571 Finger, L.W., Hazen, R.M., and Prewitt, C.T. (1991) Crystal structures of
572 $Mg_{12}Si_4O_{19}(OH)_2$ (phase B) and $Mg_{14}Si_5O_{24}$ (phase AnhB). American Mineralogist,
573 76, 1-7.

574 Ganguly, J., and Frost, D.J. (2006) Stability of anhydrous phase B: Experimental studies
575 and implications for phase relations in subducting slab and the X discontinuity in the
576 mantle. Journal of Geophysical Research, 111, B06203, 1-8.
577 Griffin, W.L., Afonso, J.C., Belousova, E.A., Gain, S.E., Gong, X.H., Gonzalez-Jimenez,
578 J.M., Howell, D., Huang, J.X., McGowan, N., Pearson, N.J., Satsukawa, T., Shi, R.,
579 Williams, P., Xiong, Q., Yang, J.S., Zhang, M., and O'Reilly, Y. (2016) Mantle
580 recycling: transition zone metamorphism of Tibetan ophiolitic peridotites and its
581 tectonic implications. Journal of Petrology, 57, 655-684.
582 Hazen, R.M. (1976) Effects of temperature and pressure on the cell dimension and
583 X-ray temperature factors of periclase. American Mineralogist, 61, 266-271.
584 Heinemann, S., Sharp, T.G., Seifert, F., and Rubie, D.C. (1997) The cubic-tetragonal
585 phase transition in the system majorite ($Mg_4Si_4O_{12}$) – pyrope ($Mg_3Al_2Si_3O_{12}$), and
586 garnet symmetry in the earth's transition zone. Physics and Chemistry of Minerals,
587 24, 206-221.
588 Herrmann, W., and Berry, R.F. (2002) MINSQ – a least squares spreadsheet method for
589 calculating mineral proportions from whole rock major element analyses.
590 Geochemistry: Exploration, Environment, Analysis, 2, 361-368.
591 Horiuchi. H., and Sawamoto, H. (1981) β-Mg_2SiO_4: Single-crystal X-ray diffraction

592 study. American Mineralogist, 66, 568-575.

593 Ishii, T., Kojitani, H., Tsukamoto, S., Fujino, K., Mori, D., Inaguma, Y., Tsujino, N.,

594 Yoshino, T., Yamazaki, D., Higo, Y., Funakoshi, K., and Akaogi, M. (2014)

595 High-pressure phase transitions in $FeCr_2O_4$ and structure analysis of new post-spinel

596 $FeCr_2O_4$ and $Fe_2Cr_2O_5$ phases with meteoritical and petrological implications.

597 American Mineralogist, 99, 1788-1797.

598 Ishii, T., Kojitani, H., Fujino, K., Yusa, H., Mori, D., Inaguma, Y., Matsushita, Y.,

599 Yamaura, K., and Akaogi, M. (2015) High-pressure high-temperature transitions in

600 $MgCr_2O_4$ and crystal structures of new $Mg_2Cr_2O_5$ and post-spinel $MgCr_2O_4$ phases

601 with implications for ultra-high pressure chromitites in ophiolites, American

602 Mineralogist, 100, 59–65.

603 Ito, E. (2007) Theory and Practice – Multianvil cells and high-pressure experimental

604 methods, In G.D. Price, Ed., Mineral Physics, 2, p. 197-230. Treatise on Geophysics,

605 Elsevier, Amsterdam.

606 Kirby, S.H., Stein, S., Okal, E.A., and Rubie, D.C. (1996) Metastable mantle phase

607 transformations and deep earthquakes in subducting oceanic lithosphere. Review of

608 Geophysics, 34, 261-306.

609 Kirfel, A., Lippmann, T., Blaha, P., Schwarz, K., Cox, D.F., Rosso, K.M., and Gibbs,

610 G.V. (2005) Electron density distribution and bond critical point properties for
611 forsterite, Mg_2SiO_4, determined with synchrotron single crystal X-ray diffraction
612 data. Physics and Chemistry of Minerals, 32, 301-313.

613 Kojitani, H., Hisatomi, R., and Akaogi, M. (2007) High-pressure phase relations and
614 crystal chemistry of calcium ferrite-type solid solutions in the system
615 $MgAl_2O_4$-Mg_2SiO_4. American Mineralogist, 92, 1112-1118, doi:
616 10.2138/am.2007.2255.

617 Kojitani, H., Enomoto, A., Tsukamoto, S., Akaogi, M., Miura, H., Yusa, H. (2010)
618 High-pressure high-temperature phase relations in $MgAl_2O_4$. Journal of Physics:
619 Conference Series, 215, 012098, doi:10.1088/1742-6596/215/1/012098.

620 Kojitani, H., Terata, S., Ohsawa, M., Mori, D., Inaguma, Y., and Akaogi, M. (2017)
621 Experimental and thermodynamic investigations on the stability of $Mg_{14}Si_5O_{24}$
622 anhydrous phase B with relevance to Mg_2SiO_4 forsterite, wadsleyite and ringwoodite.
623 American Mineralogist, in press.

624 Lenaz, D., Skogby, H., Princivalle, F., and Halenius, U. (2004) Structural changes and
625 valence states in the $MgCr_2O_4$-$FeCr_2O_4$ solid solution series. Physics and Chemistry
626 of Minerals, 31, 633-642, doi: 10.1007/s00269-004-0420-0.

627 Liou, J.G., Tsujimori, T., Yang, J., Zhang, R.Y., and Ernst, W.G. (2014) Recycling of

crustal materials through study of ultrahigh-pressure minerals in collisional orogens, ophiolites, and mantle xenoliths: A review. Journal of Asian Earth Sciences, 96, 386-420.

Miura, H., Hamada, Y., Suzuki, T., Akaogi, M., Miyajima, N., and Fujino, K. (2000) Crystal structure of $CaMg_2Al_6O_{12}$, a new Al-rich high pressure form. American Mineralogist, 85, 1799-1803.

Miyajima, N., Yagi, T., Hirose, K., Kondo, T., Fujino, K., and Miura, H. (2001) Potential host phase of aluminum and potassium in the Earth's lower mantle. American Mineralogist, 86, 740–746.

Morishima, H., Kato, T., Suto, M., Ohtani, E., Urakawa, U., Shimomura, O., and Kikegawa, T. (1994) The phase boundary between α-Mg_2SiO_4 and β-Mg_2SiO_4 determined by in situ X-ray observation. Science, 265, 1202-1203.

Ono, A., Akaogi, M., Kojitani, H., Yamashita, K. and Kobayashi, M. (2009) High-pressure phase relations and thermodynamic properties of hexagonal aluminous phase and calcium-ferrite phase in the systems $NaAlSiO_4$-$MgAl_2O_4$ and $CaAl_2O_4$-$MgAl_2O_4$. Physics of the Earth and Planetary Interiors, 174, 39–49.

Ozima, M. (1982) Growth of orthoenstatite crystals by flux method. Journal of Japanese Association of Mineralogist, Petrologist and Economic Geologist, Special Paper, 3,

97–103.

Ricolleau, A., Perrillat, J.P., Fiquet, G., Daniel, I., Matas, J., Addad, A., Menguy, N., Cardon. H., Mezouar, M., and Guignot, N. (2010) Phase relations and equation of state of a natural MORB: Implications for the density profile of subducted oceanic crust in the Earth's lower mantle. Journal of Geophysical Research, 115, B08202. doi:10.1029/2009JB006709.

Robinson, P.T., Bai, W.J., Malpas, J., Yang, J.S., Zhou, M.F., Fang, Q.S., Hu, X.F., Cameron, S., and Staudigel, H. (2004) Ultra-high pressure minerals in the Luobusa ophiolite, Tibet, and their tectonic implications. Geological Society, London, Special Publication, 226, 247–271.

Sanehira, T., Irifune, T., Shinmei, T., Ohfuji, H., Brunet, F., and Funakoshi, K. (2008) Density profiles of pyrolite and MORB compositions across the 660 km seismic discontinuity. High Pressure Research, 28, 335-349.

Satsukawa, T., Griffin, W.L., Piazolo, S., and O'Reilly, S.Y. (2015) Messengers from the deep: Fossil wadsleyite-chromite microstructure from the mantle transition zone. Scientific Reports, 5, 16484; doi:10.1038/srep16484.

Sirotkina, E.A., Bobrov, A.V., Bindi, L., and Irifune, T. (2015) Phase relations and formation of chromium-rich phases in the system $Mg_4Si_4O_{12}$-$Mg_3Cr_2Si_3O_{12}$ at 10-24

664 GPa and 1600 °C. Contributions to Mineralogy and Petrology, 169, 1-14, doi
665 10.1007/ s00410-014-1097-0.
666 Suzuki, A., Ohtani, E., Morishima, H., Kubo, T., Kanbe, Y., and Kondo, T. (2000) In situ
667 determination of the phase boundary between wadsleyite and ringwoodite in
668 Mg_2SiO_4. Geophysical Research Letters, 27, 803-806.
669 Takahashi, E. (1986) Genesis of calc-alkali andesite magma in a hydrous mantle-crust
670 boundary: Petrology of lherzolite xenoliths from the Ichinomegata crater, Oga
671 peninsula, northeast Japan, Part II. Journal of Volcanology and Geothermal Research,
672 29, 355-395.
673 Withers, A.C., Essene, E.J., and Zhang, Y. (2003) Rutile/TiO_2II phase equilibria.
674 Contributions to Mineralogy and Petrology, 145, 199-204.
675 Wu, Y., Xu, M., Jin, Z., Fei, Y., and Robinson, P.T. (2016) Experimental constraints on
676 the formation of the Tibetan podiform chromitites. Lithos, 245, 109-117.
677 Yamamoto, S., Kojima, T., Hirose, K., Maruyama, S. (2009) Coesite and clinopyroxene
678 exsolution lamella in chromites: *In-situ* ultrahigh-pressure evidence from podiform
679 chromitites in the Luobusa ophiolite, southern Tibet. Lithos, 109, 314-322.
680 Yang, J.S., Dorbrzhinetskaya, L., Bai, W.J., Fang, Q.S., Robinson, P.T., Zhang, J., and
681 Green II, H.W. (2007) Diamond- and coesite-bearing chromitites from the Luobusa

ophiolite, Tibet. Geology, 35, 875-878, doi: 10.1130/G23766A.

Yang, J.S., Meng, F.C., Xu, X.Z., Robinson, P.T., Dilek, Y., Makeyev, A.B., Wirth, R., Wiedenbeck, M., Griffin, W.L., and Cliff, J. (2015) Diamonds, native elements and metal alloys from chromitites of the Ray-Iz ophiolite of the Polar Urals. Gondwana Research 27, 459–485.

Zhang, J., Li, B., Utsumi, W., and Liebermann, R.C. (1996) In situ X-ray observations of the coesite-stishovite transition: reversed phase boundary and kinetics. Physics and Chemistry of Minerals, 23, 1-10.

Zhang, R.Y., Yang, J.S., Ernst, W.G., Jahn, B.M., Iizuka, Y., and Guo, G.L. (2016) Discovery of in situ super-reducing, ultrahigh-pressure phases in the Luobusa ophiolitic chromitites, Tibet: New insights into the deep upper mantle and mantle transition zone. American Mineralogist, 101, 1285-1294.

Zhang, Y., Jin, Z., Griffin, W.L., Wang, C., and Wu, Y. (2017) High-pressure experiments provide insights into the mantle transition zone history of chromitite in Tibetan ophiolites. Earth and Planetary Science Letters, 463, 151-158.

699 **Figure captions**

700

701 **Figure 1**. Microfocus X-ray diffraction patterns of the run products at 1600 °C at (a)
702 12.5 GPa and (b) 16 GPa. Ol: olivine, Ch: chromite, Gt: garnet, mLd: modified
703 ludwigite phase, B: anhydrous phase B.

704

705 **Figure 2**. Microfocus X-ray diffraction patterns of the run products at 1600 °C at (a)
706 20.5 GPa, (b) 22.5 GPa and (c) 27 GPa. Gt: garnet, mLd: modified ludwigite phase,
707 Wd: wadsleyite, Rw: ringwoodite, CT: calcium-titanate phase, Brg: bridgmanite
708 (perovskite), Per: periclase, Pt: platinum.

709

710 **Figure 3**. Back-scattered electron images of the run products at (a) 12.5GPa, (b) 19 GPa,
711 (c) 20.5 GPa, (d) 22.5 GPa, and (e) 27 GPa. In (a), the light and dark gray grains are
712 chromite (Ch) and olivine (Ol), respectively. In (b), white grains are modified ludwigite
713 (mLd) phase, light gray grains are garnet (Gt), and dark gray grains are anhydrous phase
714 B (Anh-B). In (c), white grains are mLd, light gray grains are Gt, and dark gray grains
715 are wadsleyite (Wd). In (d), light gray grains are calcium-titanate (CT) phase and dark
716 gray grains are ringwoodite (Rw). In (e), light gray grains are CT, dark gray grains are

717 bridgmanite (Brg), and small, most dark gray grains are periclase (Per).

718

719 **Figure 4**. Compositions of coexisting phases in triangular diagrams of the
720 $MgO–SiO_2–Cr_2O_3$ system (mol%). The circles represent the compositions of
721 endmember phases, and the small triangle marks the starting material composition
722 (50mol%Mg_2SiO_4·50mol%$MgCr_2O_4$). The compositions of all endmember phases are
723 shown in (a). The phases coexisting at high pressures at 1600 °C are: (b) Ol + Ch, (c) Gt
724 + mLd + Anh-B, (d) Gt + mLd + Wd, (e) Rw + CT, and (f) Brg + Per + CT. The small
725 open diamond in (b) and (c) shows the approximate composition of the starting material
726 of Wu et al. (2016), see text. The abbreviations are the same as those in Figs. 1 and 2.

727

728 **Figure 5**. Mineral proportions of the bulk composition of Mg_2SiO_4·$MgCr_2O_4$ as a
729 function of pressure at 1600 °C. The small dots indicate the mineral proportions
730 calculated based on the compositions in Table 2. The gray zones represent the pressure
731 ranges of the transition between low- and high-pressure phase assemblages. The
732 abbreviations are the same as those in Figs. 1 and 2.

733

734

This is a preprint, the final version is subject to change, of the American Mineralogist (MSA)
Cite as Authors (Year) Title. American Mineralogist, in press.
DOI: http://dx.doi.org/10.2138/am-2018-6135

Table 1. Results of high-pressure high-temperature experiments in the system Mg_2SiO_4–$MgCr_2O_4$.

Run no.	Start. Mater.	Pressure (GPa)	Temperature (°C)	Time (min)	Phases
K151104	A	9.5	1600	180	Ol + Ch
K151130	A	11.5	1600	360	Ol + Ch
A140704	A	12.5	1600	180	Ol + Ch
K160113	B	12.5	1600	360	Ol + Ch
A140801	A	14	1600	180	Gt + mLd + Anh-B
Y161025	B	14	1600	360	Gt + mLd + Anh-B
Y170525	B	16	1600	180	Gt + mLd + Anh-B
K151222	B	18	1600	180	Gt + mLd + Anh-B
Y161017	B	19	1600	360	Gt + mLd + Anh-B
Y161125	B	20.5	1600	180	Gt + mLd + Wd
A141104	A	21.5	1600	360	Rw + CT
K151118	A	22.5	1600	180	Rw + CT
K151126	A	24	1600	180	Brg + Per + CT
K150904	A	27	1600	300	Brg + Per + CT
Y160117	B10	15	1600	180	Gt + Anh-B + Wd
Y160119	B70	15	1600	180	Gt + mLd + Es

Starting materials. A: a mixture of Mg_2SiO_4 forsterite and $MgCr_2O_4$ magnesiochromite with 1:1 molar ratio, B: a mixture of MgO, SiO_2 and Cr_2O_3 with 3:1:1 molar ratio, equivalent to A composition, B10: a mixture of MgO, SiO_2 and Cr_2O_3 with 19:9:1 molar ratio, equivalent to 90mol%Mg_2SiO_4·10mol%$MgCr_2O_4$, and B70: a mixture of MgO, SiO_2 and Cr_2O_3 with 13:3:7 molar ratio, equivalent to 30mol%Mg_2SiO_4 ·70mol%$MgCr_2O_4$.

Abbreviations. Ol: olivine, Ch: chromite, Gt: garnet, mLd: modified ludwigite phase, Anh-B: anhydrous phase B, Wd: wadsleyite, Rw: ringwoodite, CT: calcium-titanate phase, Brg: bridgmanite (perovskite), Per: periclase, Es: eskolaite.

767

Table 2. Compositions of coexisting phases in the run products.

Run no.	K151104			K160113			A140704			Y161025				A140801			
P (GPa)	9.5			12.5			12.5			14				14			
Phase	Ol	Ch		Ol	Ch		Ol	Ch		Anh-B	Gt	mLd		Anh-B	Gt	mLd	
SiO_2	41.09(42)	2.47(22)		42.18(36)	1.91(36)		42.23(69)	2.32(33)		29.96(32)	43.37(76)	1.06(22)		30.86(22)	42.88(135)	0.76(16)	
MgO	57.01(60)	22.35(59)		57.09(48)	24.42(79)		56.46(82)	21.42(34)		55.31(48)	29.16(52)	35.35(67)		55.27(105)	28.80(132)	32.81(105)	
Cr_2O_3	2.14(8)	74.89(79)		1.31(15)	73.47(75)		1.52(20)	76.81(126)		14.59(35)	26.92(82)	63.59(146)		13.27(76)	25.35(113)	67.76(136)	
Total (wt%)	100.24	99.71		100.58	99.80		100.21	100.55		99.86	99.45	100.00		99.40	97.03	101.33	
O	4	4		4	4		4	4		24	12	5		24	12	5	
Si	0.97(1)	0.08(1)		0.99(1)	0.06(1)		0.99(1)	0.07(1)		4.50(4)	3.21(3)	0.04(1)		4.64(7)	3.24(5)	0.03(1)	
Mg	2.00(1)	1.05(3)		1.99(1)	1.14(3)		1.98(1)	1.02(4)		12.39(6)	3.22(5)	2.02(4)		12.38(3)	3.26(3)	1.87(3)	
Cr	0.04(1)	1.86(2)		0.03(1)	1.82(2)		0.03(1)	1.90(2)		1.73(3)	1.58(5)	1.93(4)		1.58(7)	1.50(7)	2.05(2)	
Cation total	3.01	2.99		3.01	3.02		3.00	2.99		18.62	8.01	3.99		18.60	8.00	3.95	

Run no.	Y170525			K151222			Y161017			Y161125		
P (GPa)	16			18			19			20.5		
Phase	Anh-B	Gt	mLd	Anh-B	Gt	mLd	Anh-B	Gt	mLd	Wd	Gt	mLd
SiO_2	26.01(35)	43.94(52)	0.71(21)	27.24(33)	45.48(79)	1.35(15)	28.43(60)	47.58(64)	1.09(65)	41.75(48)	47.46(67)	2.33(47)
MgO	53.70(45)	29.04(56)	31.88(58)	55.02(63)	31.30(70)	35.47(98)	56.70(67)	31.16(46)	36.33(74)	52.55(50)	31.88(56)	35.17(48)
Cr_2O_3	19.76(46)	26.74(79)	66.97(71)	17.44(62)	23.57(30)	61.00(39)	15.42(45)	21.27(52)	62.62(86)	5.78(28)	20.15(59)	62.80(64)
Total (wt%)	99.47	99.72	99.56	99.70	100.35	97.82	100.55	100.01	100.04	100.08	99.49	100.30
O	24	12	5	24	12	5	24	12	5	4	12	5
Si	4.01(5)	3.24(4)	0.03(1)	4.16(5)	3.30(3)	0.05(1)	4.27(7)	3.42(3)	0.04(2)	0.99(1)	3.42(3)	0.09(2)
Mg	12.36(10)	3.19(5)	1.85(3)	12.52(7)	3.38(6)	2.07(4)	12.71(10)	3.34(4)	2.07(4)	1.86(1)	3.43(5)	1.99(3)
Cr	2.41(5)	1.56(5)	2.06(2)	2.11(6)	1.35(3)	1.89(2)	1.83(6)	1.21(3)	1.90(4)	0.11(1)	1.15(4)	1.89(2)
Cation total	18.78	7.99	3.94	18.79	8.03	4.01	18.81	7.97	4.01	2.96	8.00	3.97

Run no.	A141104			K151118			K151126			K150904		
P (GPa)	21.5			22.5			24			27		
Phase	Rw	CT		Rw	CT		Brg	CT		Brg	CT	
SiO_2	41.46(26)	1.87(12)		40.56(78)	4.96(24)		55.08(84)	5.79(22)		55.62(62)	6.80(71)	
MgO	56.70(22)	22.41(32)		52.99(35)	24.17(58)		37.54(139)	25.47(63)		39.12(106)	28.15(33)	
Cr_2O_3	1.83(10)	75.33(46)		6.24(35)	70.54(66)		7.19(42)	68.75(53)		5.40(72)	64.74(101)	
Total (wt%)	99.99	99.61		99.79	99.67		99.81	100.01		100.14	99.69	
O	4	4		4	4		3	4		3	4	
Si	0.98(1)	0.06(1)		0.97(1)	0.15(1)		0.95(1)	0.18(1)		0.95(1)	0.20(2)	
Mg	1.98(1)	1.05(1)		1.89(2)	1.11(2)		0.96(3)	1.16(2)		1.00(2)	1.27(1)	
Cr	0.03(1)	1.89(1)		0.12(1)	1.72(2)		0.10(1)	1.66(2)		0.08(1)	1.55(3)	
Cation total	2.99	3.00		2.98	2.98		2.01	3.00		2.03	3.02	

Ol: olivine, Ch: chromite, Gt: garnet, mLd: modified ludwigite phase, Anh-B: anhydrous phase B, Wd: wadsleyite, Rw: ringwoodite,
CT: calcium-titanate phase, Brg: bridgmanite (perovskite).

768

769

770

This is a preprint, the final version is subject to change, of the American Mineralogist (MSA)
Cite as Authors (Year) Title. American Mineralogist, in press.
DOI: http://dx.doi.org/10.2138/am-2018-6135

Table 3. Molar volumes of phases in the system MgO-SiO_2-Cr_2O_3.

Phase	Composition	V_0 (cm^3/mol)	Ref.
Ol	Mg_2SiO_4	43.59	Kirfel et al. (2005)
Wd	Mg_2SiO_4	40.52	Horiuchi and Sawamoto (1981)
Rw	Mg_2SiO_4	39.53	Akaogi et al. (1989)
CT	Mg_2SiO_4	36.49	Kojitani et al. (2007), see text
Brg	$MgSiO_3$	24.25	Dobson and Jacobson (2004)
Ch	$MgCr_2O_4$	43.56	This study
CT	$MgCr_2O_4$	39.42	Ishii et al. (2015)
Gt	$Mg_4Si_4O_{12}$	113.86	Heinemann et al. (1997), see text
Gt	$Mg_3Cr_2Si_3O_{12}$	117.58	Sirotkina et al. (2015), see text
Anh-B	$Mg_{14}Si_5O_{24}$	251.75	Finger et al. (1991)
mLd	$Mg_2Cr_2O_5$	51.61	Ishii et al. (2015)
Per	MgO	11.24	Hazen (1976)

Ol: olivine, Wd: wadsleyite, Rw: ringwoodite, CT: calcium-titanate type phase, Brg: bridgmanite (perovskite), Ch: chromite, Gt: garnet, Anh-B: anhydrous phase B, mLd: modified ludwigite phase, Per: periclase.

This is a preprint, the final version is subject to change, of the American Mineralogist (MSA)
Cite as Authors (Year) Title. American Mineralogist, in press.
DOI: http://dx.doi.org/10.2138/am-2018-6135

Fig. 1

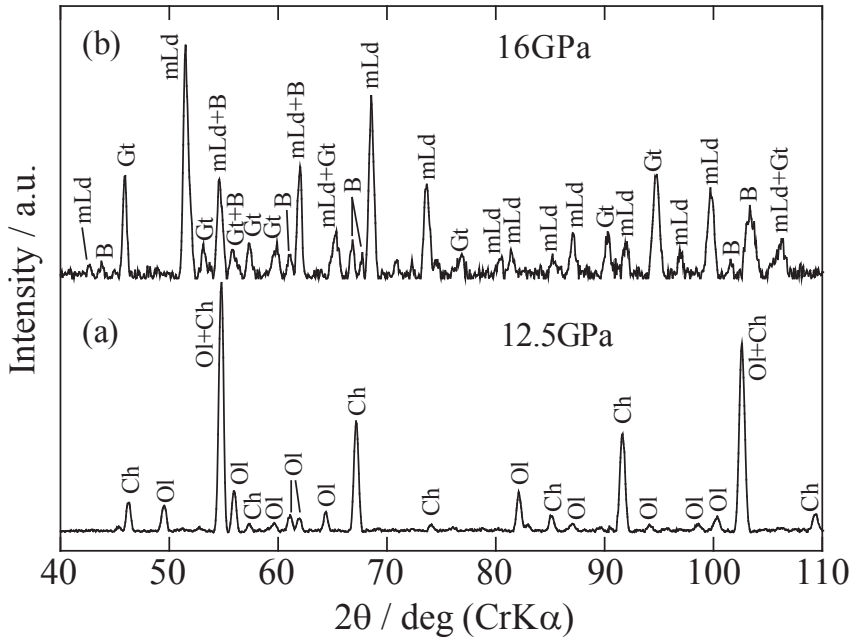

This is a preprint, the final version is subject to change, of the American Mineralogist (MSA)
Cite as Authors (Year) Title. American Mineralogist, in press.
DOI: http://dx.doi.org/10.2138/am-2018-6135

Fig. 2.

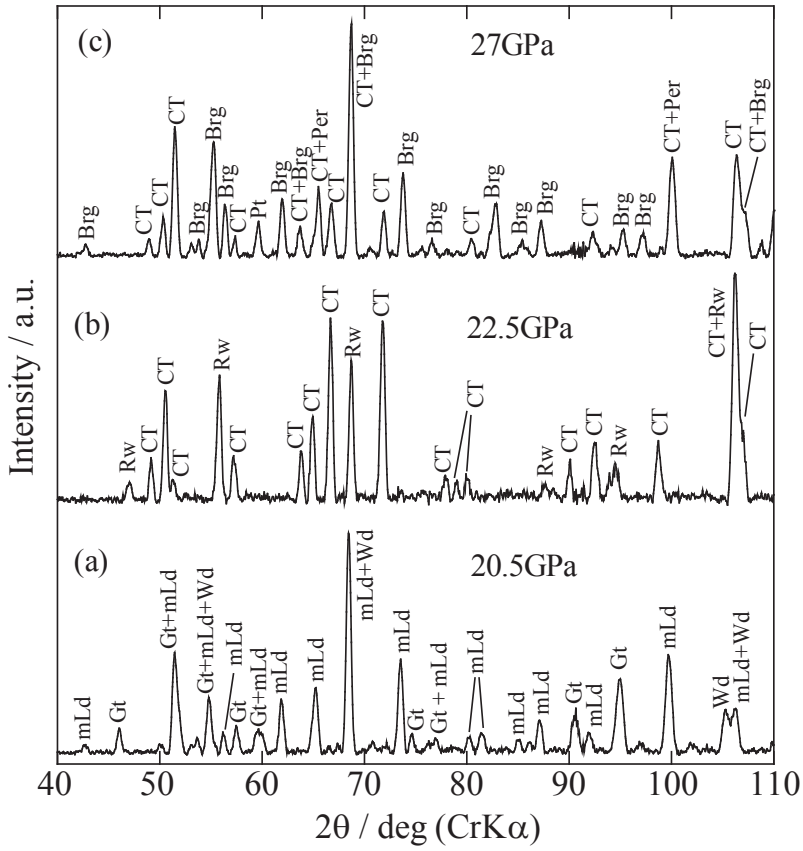

This is a preprint, the final version is subject to change, of the American Mineralogist (MSA)
Cite as Authors (Year) Title. American Mineralogist, in press.
DOI: http://dx.doi.org/10.2138/am-2018-6135

Fig. 3

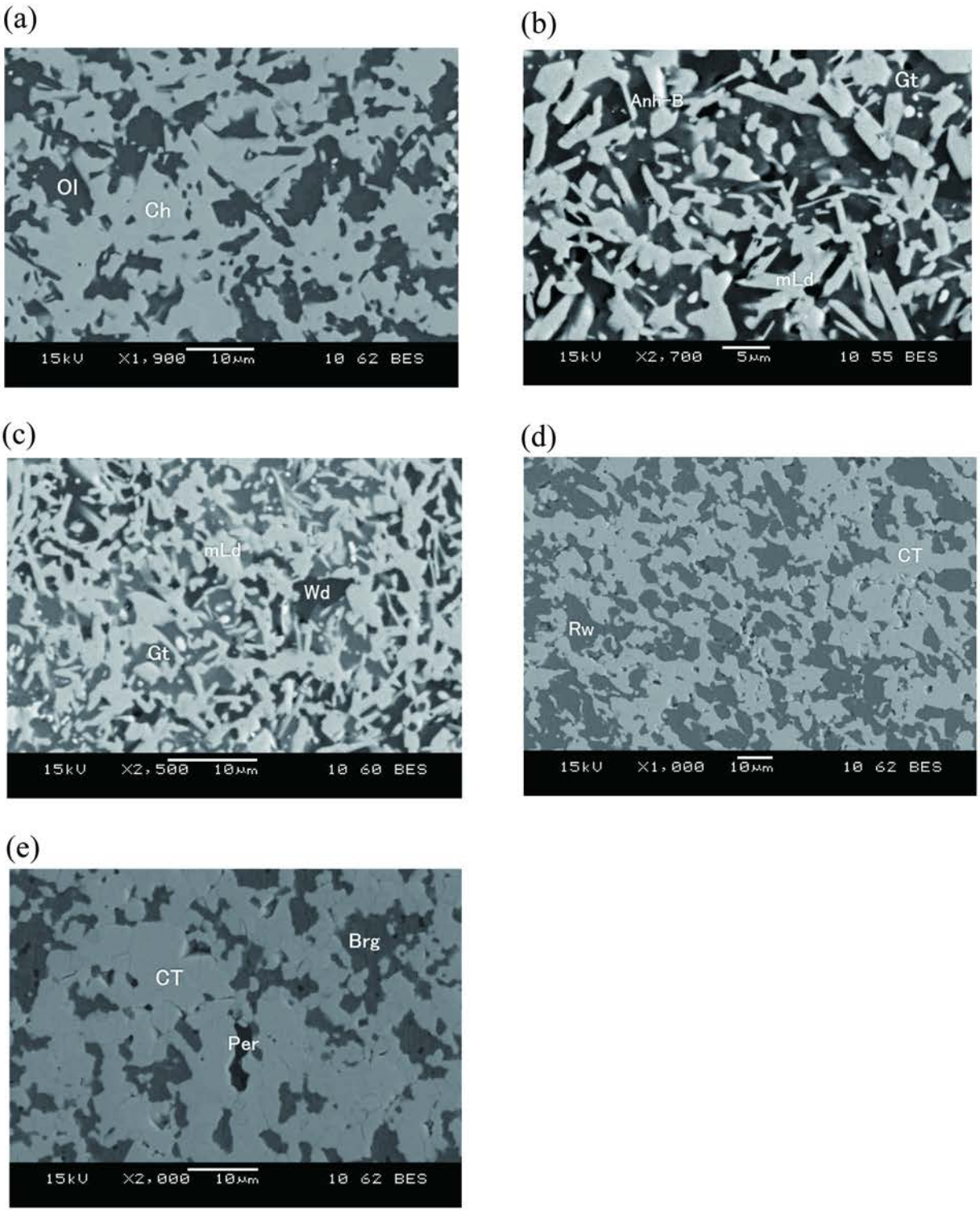

This is a preprint, the final version is subject to change, of the American Mineralogist (MSA)
Cite as Authors (Year) Title. American Mineralogist, in press.
DOI: http://dx.doi.org/10.2138/am-2018-6135

Fig. 4

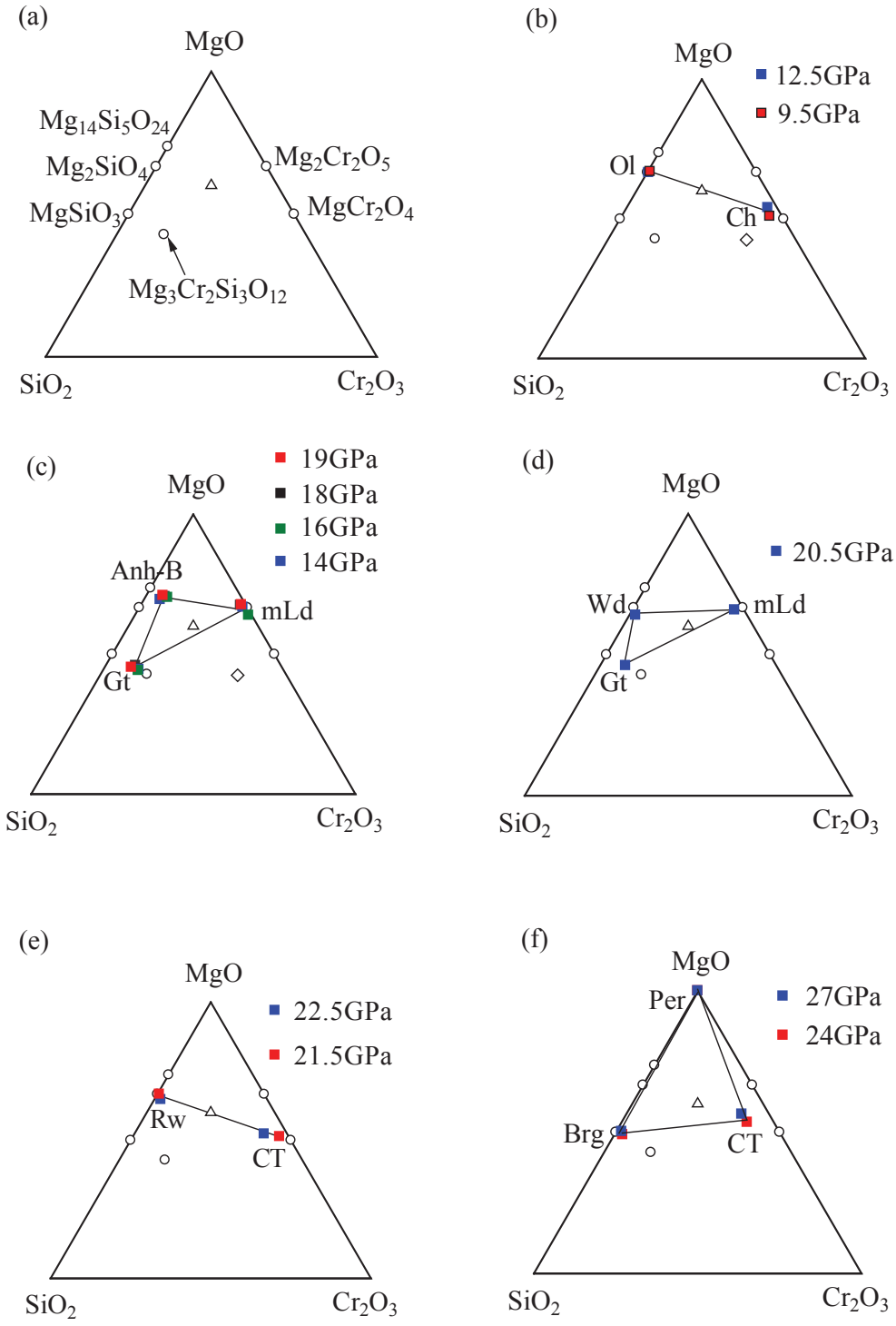

This is a preprint, the final version is subject to change, of the American Mineralogist (MSA)
Cite as Authors (Year) Title. American Mineralogist, in press.
DOI: http://dx.doi.org/10.2138/am-2018-6135

Figure 5